Distributed-feedback terahertz quantum-cascade lasers with laterally corrugated metal waveguides

Benjamin S. Williams, Sushil Kumar, and Qing Hu

Department of Electrical Engineering and Computer Science and Research Laboratory of Electronics, Massachusetts Institute of Technology, Cambridge, Massachusetts 02139

John L. Reno

Sandia National Laboratories, Department 1123, MS 0601, Albuquerque, New Mexico 87185-0601

Received May 27, 2005; revised manuscript received July 7, 2005; accepted July 9, 2005

We report the demonstration of distributed-feedback terahertz quantum-cascade lasers based on a first-order grating fabricated via a lateral corrugation in a double-sided metal ridge waveguide. The phase of the facet reflection was precisely set by lithographically defined facets by dry etching. Single-mode emission was observed at low to moderate injection currents, although multimode emission was observed far beyond threshold owing to spatial hole burning. Finite-element simulations were used to calculate the modal and threshold characteristics for these devices, with results in good agreement with experiments. © 2005 Optical Society of America

OCIS codes: 140.3070, 140.5960, 140.3490, 230.5590.

Terahertz quantum-cascade lasers (QCLs) are poised to play a large role in the growing field of terahertz science and technology ($f \sim 1-10$ THz, $\sim 30-300$ μm).[1–3] Perhaps the most immediate application for terahertz QCLs is as local oscillators in heterodyne receiver systems above 2 THz.[4] While only microwatts of optical power are needed to pump superconducting mixers, stable, narrow-linewidth, single-mode operation is required. For mid-infrared QCLs, single-mode operation is typically accomplished using a distributed-feedback (DFB) grating, where index or gain–loss modulation is introduced via etching into the upper waveguide cladding or gain region, sometimes in combination with a metallized grating.[5] Recently, a corrugated lateral grating fabricated using high-aspect-ratio dry etching was demonstrated for a QCL operating at 11 μm.[6] The use of lateral distributed feedback allowed the grating to be defined lithographically and to be decoupled from the design of the vertical waveguiding structure and epitaxial growth.

In this Letter we report the demonstration of first-order DFB terahertz QCLs fabricated using lateral corrugation in a metal–metal ridge waveguide. In this type of waveguide, metal layers are placed on either side of the 10 μm thick epitaxial active region.[7] This waveguide is similar in form to a microstrip transmission line and displays extremely strong subwavelength modal confinement in both the vertical and the lateral dimensions.[8] It should be noted that this waveguide is different from the other surface-plasmon waveguide commonly used in terahertz QCLs, where the mode extends into the undoped substrate[1] and for which loss-coupled DFB QCLs have been demonstrated.[9,10]

The active region was based on the resonant-phonon depopulation concept, in a design similar to that described in Ref. 11. Following growth of the sample (labeled FL176C-M4-2) by molecular beam epitaxy, the metal–metal waveguide was fabricated using a copper-to-copper thermocompression wafer bonding technique as described in Ref. 3. Following wafer bonding and substrate removal, corrugated Ti–Au metal contacts (20/500 nm) were defined on the 10 μm thick epitaxial active region by contact lithography. The corrugated ridge waveguides were then defined by dry etching by use of the top metallic contact as a self-aligned etch mask,[3] and the receptor substrate was lapped to 180 μm.

DFB lasers are often designed with antireflection coatings to prevent reflections from the cleaved facets from competing with the grating feedback, which can alter the relative lasing thresholds of various modes and cause lasing of unwanted modes. The precise effect is related to the phase $\sim 2\pi l/\Lambda$ of the effective complex facet reflectivity, where l is the facet length with respect to grating period Λ [see Fig. 1(b)]. The problem is potentially more severe in the terahertz region, as antireflection coatings are more difficult to fabricate. Furthermore, due to the impedance mismatch between free space and the tightly confined subwavelength mode, metal–metal waveguides have much larger cleaved facet reflectivities ($R \sim 0.7-0.9$ for a 10 μm thick active region) than would be expected from the GaAs–air index mismatch ($R = 0.32$).[8] However, because of the longer wavelength of terahertz radiation it is feasible to define the waveguide facet (and its reflectivity phase) in a controllable way by using dry etching [Fig. 1(a)].

For testing, the device was indium soldered onto a copper chip carrier in a vacuum cryostat, and wire bonds were made directly on top of the corrugated ridges. The ridges were 49 μm wide at the widest sections, with 10 μm lateral corrugations in either side, and a corrugation duty cycle of approximately 44%.

0146-9592/05/212909-3/$15.00

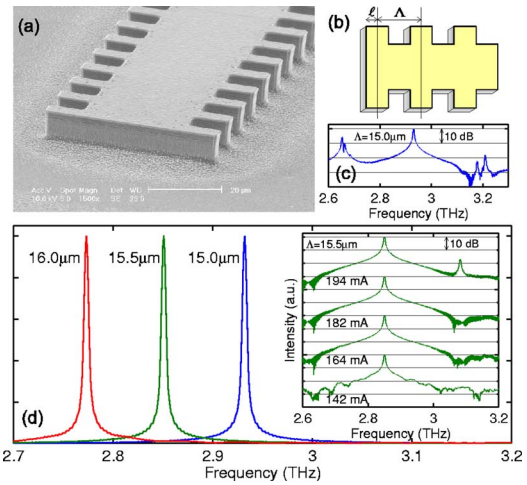

Fig. 1. (a) (Online color) Metal–metal corrugated ridge DFB with (b) dry-etched facets of extension length l. (c) Spectrum from a $\Lambda=15.0$ μm, $l=-\Lambda/4$ device at high bias. (d) Spectra from DFB devices with several grating periods Λ, with $l=\Lambda/4$ taken at 8 K at moderate bias. Inset, spectra taken at multiple biases from the $\Lambda=15.5$ μm device.

All ridges were roughly 1.0 mm long. Spectra were taken under a nitrogen gas purge with a Nicolet Fourier-transform spectrometer (resolution, 3.75 GHz).

Devices were tested for several facet lengths and several grating periods. At low bias, single-mode behavior was observed for most devices, but some of the best results were obtained from devices with a facet length of $l=\Lambda/4$. Continuous-wave spectra taken at a moderate injection current at a heat-sink temperature of 8 K from three devices with $\Lambda=15.0$, 15.5, 16.0 μm are shown in Fig. 1(d). These devices lased at 2.935, 2.853, and 2.776 THz, respectively, which scales well with the grating period. For comparison, Fabry–Perot devices fabricated from the same wafer tended to lase at 2.7–2.85 THz. The peak power emitted from the DFB devices was relatively low (100–300 μW per facet) in comparison to that from similar Fabry–Perot devices, which emit ~1 mW.

As the bias was increased far beyond threshold, most devices lased in additional modes owing to spatial hole burning, as can be seen in the spectra shown in the inset of Fig. 1(d) taken from the device with $\Lambda=15.5$ μm, with a facet extension of $l=2.9$ μm. As is discussed below, the principal mode at 2.853 THz and the higher-frequency mode at 3.085 THz can be associated with the edges of the grating stop band, which corresponds to a bandgap of approximately $\Delta f=0.23$ THz. Stop bands of similar magnitude ($\Delta f=0.21$ THz for $\Lambda=15.0$ μm, $\Delta f=0.25$ THz for $\Lambda=16.0$ μm) were observed for devices with different grating periods. The size of the stop band can be used to estimate coupling coefficient κ used in the coupled-wave model[12] according to $|\kappa|=\pi n_{\mathrm{eff}}\Delta f/c$, where the effective refractive index is $n_{\mathrm{eff}}=\lambda_B/2\Lambda\approx 3.26$ and λ_B is the Bragg wavelength taken at the center of the observed stop band. This expression gives the value $|\kappa|\approx 79$ cm^{-1}, which indicates a much stronger grating than expected from the usual estimate of $\kappa\approx 2\Delta n_{\mathrm{eff}}/\lambda_0=23$ cm^{-1}, where $\Delta n_{\mathrm{eff}}=0.12$ is the difference in effective indices in the wide and narrow regions of the waveguide. However, this perturbative calculation fails because the surface-plasmon modes are strongly coupled to the metallic corrugation, and thus a large discontinuity in the dielectric constant is seen at each grating step. An additional high bias spectrum from a $\Lambda=15.0$ μm, $l=-\Lambda/4$ device is plotted in Fig. 1(c), which supports modes separated by 0.55 THz. This large gain bandwidth suggests the potential for wide tunability if the gain medium is placed in a tunable cavity.

Single-mode behavior over the entire bias range was observed in a different device with $\Lambda=15$ μm and $l=6.75$ μm. The collected single-facet optical power is plotted in Fig. 2 versus current for several heat-sink temperatures. In continuous-wave operation, the threshold current density for this device was 370 A/cm^2 at 8 K, and it lased up to a heat-sink temperature of 97 K, over which 12 GHz of temperature tuning was obtained.

A more comprehensive picture of DFB operation was obtained by performing full-wave three-dimensional finite-element[13] simulations for a $\Lambda=15.5$ μm device with $l=2.9$ μm, which corresponds to the device whose testing is shown in Fig. 1(d). Because of memory limitations, only a device 465 μm in length could be simulated. Furthermore, the longitudinal and lateral symmetry of the problem was used to reduce the scale of the problem, so in fact only one quarter of the structure was truly simulated. The resonance frequencies and threshold material gains g_{th} for the various DFB modes are plotted in Fig. 3. The metal was treated as a perfect conductor and the semiconductor was undoped, so g_{th} reflects only radiative losses and not free-carrier waveguide losses (expected to be ~10 cm^{-1}). Figure 3(a) displays those modes that are laterally symmetric, and Fig. 3(b) displays the laterally antisymmetric modes. Coupled-mode analysis suggests that the results for a longer device ($L=1$ mm as tested) should be qualitatively similar to the simulated results, and indeed there is good agreement between the observed lasing modes (2.85 and 3.09 THz) and the lower and upper band-

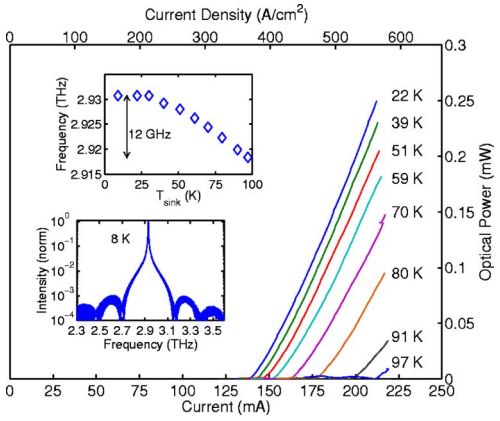

Fig. 2. (Online color) Continuous-wave optical power versus current for a device with $\Lambda=15.0$ μm and $l=6.75$ μm, which lased in a single mode over (bottom inset) the entire bias range. Upper inset, the frequency tuning achieved by changing the heat-sink temperature.

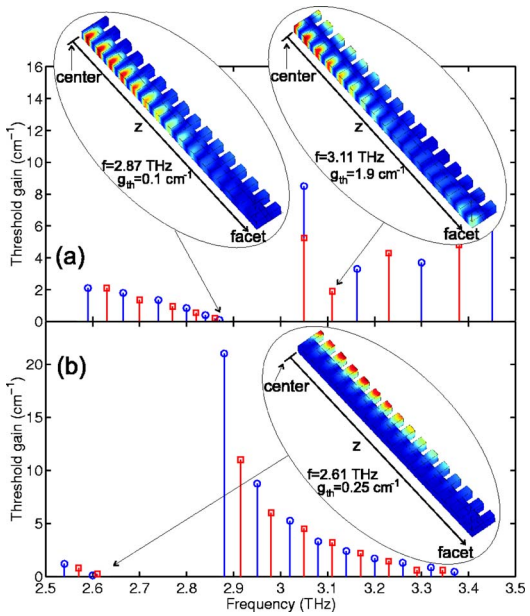

Fig. 3. (Online color) Modal threshold gains calculated by use of a three-dimensional finite-element solver for a $\Lambda = 15.5\ \mu$m, 465 μm long DFB structure with $l = 2.9\ \mu$m. Modes with even and odd lateral symmetry are shown in (a) and (b), respectively, and modes with even and odd longitudinal symmetry are marked by squares and circles, respectively. Also shown are the magnitude-squared electric field E_y plots calculated for the band edge modes (note that only one quarter of the waveguide is plotted).

edge symmetric modes at 2.87 THz ($g_{th} = 0.1$ cm^{-1}) and 3.11 THz ($g_{th} = 1.9$ cm^{-1}) respectively. The low-threshold modes with odd lateral symmetry [Fig. 3(b)] do not lase for devices with $\Lambda = 15.5\ \mu$m because they are too far away from the gain peak; however, they were observed in spectra from some $\Lambda = 15.0\ \mu$m devices [Fig. 1(c)]. Although the $l = \Lambda/4$ facet location is nominally in phase with the grating, the effective facet reflectivity is somewhat out of phase with that of the grating because the facet was fabricated shorter (2.9 μm) than its designed length and also because of a residual phase shift at the facet of the metal–metal waveguide. These effects break the symmetry across the bandgap: The upper modes couple more strongly to the facets and thus have higher g_{th}, while the modes on the lower bandgap edge maintain lower thresholds.

Examination of the modal field patterns in Fig. 3(a) reveals that the band edge modes are highly localized in the center of the waveguide, which accounts for their low measured power levels, and is consistent with the understanding that nonuniform longitudinal field profiles accompany κL products larger than unity (L is the cavity length).[12] For this simulated case $\kappa L \sim 4$; for the experimental case $L = 1$ mm and $\kappa L \sim 8$, which suggests that the longitudinal mode profiles are even more localized than in the simulated case and that these devices might be vulnerable to spatial hole burning. However, given the similarity of the longitudinal mode envelopes of the upper and lower stop band modes, the appearance of the upper mode is more likely due to spatial hole burning on the scale of the wavelength, since $\Lambda/2$ is more than an order of magnitude larger than the diffusion length associated with the intersubband population inversion (~200 nm). Finally, even though we see good agreement with simulations, we cannot completely exclude the possibility that localized modes can form about unintentional grating disorder, such as the wire bond attachment points.

The ability to easily customize the grating corrugation and facet phase conditions via lithography allows the engineering of the relative gain thresholds and longitudinal mode profiles. For example, longitudinal field uniformity and output power levels could be improved by reducing the corrugation depth (or device length) to reduce the κL product. Although this possibility is not explored here, power could be coupled preferentially out of a single facet by introducing controlled phase shifts into the length of the DFB or by independently adjusting the facet phases.

This research is supported by the AFOSR, NASA, and the NSF. Sandia Laboratories is a multiprogram laboratory operated by Sandia Corporation, a Lockheed Martin Company, for the U.S. Department of Energy under contract DE-AC04-94AL85000. B. S. Williams's e-mail address is bwilliam@mit.edu.

References

1. R. Köhler, A. Tredicucci, F. Beltram, H. E. Beere, E. H. Linfield, A. G. Davies, D. A. Ritchie, R. C. Iotti, and F. Rossi, Nature **417**, 156 (2002).
2. L. Ajili, G. Scalari, J. Faist, H. Beere, E. Linfield, D. Ritchie, and G. Davies, Appl. Phys. Lett. **85**, 3986 (2004).
3. B. S. Williams, S. Kumar, Q. Hu, and J. L. Reno, Opt. Express **13**, 3331 (2005).
4. J. R. Gao, J. N. Hovenier, Z. Q. Yang, J. J. A. Baselmans, A. Baryshev, M. Hajenius, T. M. Klapwijk, A. J. L. Adam, T. O. Klaassen, B. S. Williams, S. Kumar, Q. Hu, and J. L. Reno, Appl. Phys. Lett. **86**, 244104 (2005).
5. C. Gmachl, A. Straub, R. Colombelli, F. Capasso, D. L. Sivco, A. M. Sergent, and A. Y. Cho, IEEE J. Quantum Electron. **38**, 569 (2002).
6. S. Golka, C. Pflügl, W. Schrenk, and G. Strasser, Appl. Phys. Lett. **86**, 111103 (2005).
7. B. S. Williams, S. Kumar, H. Callebaut, Q. Hu, and J. L. Reno, Appl. Phys. Lett. **83**, 2124 (2003).
8. S. Kohen, B. S. Williams, and Q. Hu, J. Appl. Phys. **97**, 053106 (2005).
9. L. Mahler, R. Köhler, A. Tredicucci, F. Beltram, H. E. Beere, E. H. Linfield, D. A. Ritchie, and A. G. Davies, Appl. Phys. Lett. **84**, 5446 (2004).
10. L. Ajili, J. Faist, H. Beere, D. Ritchie, G. Davies, and E. Linfield, Electron. Lett. **41**, 53 (2005).
11. S. Kumar, B. S. Williams, S. Kohen, Q. Hu, and J. L. Reno, Appl. Phys. Lett. **84**, 2494 (2004).
12. H. Kogelnik and C. V. Shank, J. Appl. Phys. **43**, 2327 (1972).
13. FEMLAB 3.1, Comsol, Inc., www.comsol.com.